Crystal Structure and Antiferromagnetic Order in $NdFeAsO_{1-x}F_x$ ($x = 0.0$ and 0.2) Superconducting Compounds from Neutron Diffraction Measurements

Y. Qiu,[1,2] Wei Bao,[3,*] Q. Huang,[1] T. Yildirim,[1] J. M. Simmons,[1,2] M. A. Green,[1,2] J. W. Lynn,[1] Y. C. Gasparovic,[1,2] J. Li,[1,2] T. Wu,[4] G. Wu,[4] and X. H. Chen[4]

[1]*NIST Center for Neutron Research, National Institute of Standards and Technology, Gaithersburg, Maryland 20899, USA*
[2]*Department of Materials Science and Engineering, University of Maryland, College Park, Maryland 20742, USA*
[3]*Los Alamos National Laboratory, Los Alamos, New Mexico 87545, USA*
[4]*Hefei National Laboratory for Physical Science at Microscale and Department of Physics, University of Science and Technology of China, Hefei, Anhui 230026, China*

(Received 8 July 2008; published 17 December 2008)

The transition temperature $T_C \approx 26$ K of the recently discovered superconductor $LaFeAsO_{1-x}F_x$ is extremely sensitive to the lanthanide ion, reaching 55 K for the Sm containing oxypnictides. Therefore, it is important to determine how the moment on the lanthanide affects the overall magnetism in these systems. Here we report a neutron diffraction study of the Nd oxypnictides. Long-ranged antiferromagnetic order is apparent in NdFeAsO below 1.96 K. Rietveld refinement shows that both Fe and Nd magnetic ordering are required to describe the observed data with the staggered moment $1.55(4)\mu_B$/Nd and $0.9(1)\mu_B$/Fe at 0.3 K. The other structural properties such as the tetragonal-orthorhombic distortion are found to be very similar to those in LaFeAsO. Neither the magnetic ordering nor the structural distortion occur in the superconducting sample $NdFeAsO_{0.80}F_{0.20}$ at any temperatures down to 1.5 K.

DOI: 10.1103/PhysRevLett.101.257002 PACS numbers: 74.25.Ha, 61.05.fm, 74.70.−b, 75.30.Fv

The surprising discovery of high-T_C superconductivity in cuprates two decades ago has shifted attention to laminar magnetic materials for new high-T_C superconductors. New superconductors have been discovered since then in layered ruthenate [1] and triangular materials [2–4]. While these discoveries broke new ground for physics, their T_C's are not high. The recent discovery of high-T_C superconductors in the quaternary Fe oxypnictides $LnFeAsO_{1-x}F_x$ has revitalized the field [5–14], and the question naturally arises as to how the new family of iron-based superconductors compare to the cuprates. Parent compounds of the new superconductors share a similar electronic structure with all five d orbitals of the Fe contributing to a low density of states at the Fermi level [15–22]. This contrasts with cuprates in which parent compounds are Mott insulators with well-defined local magnetic moments [23]. On the other hand, the doping phase diagram of the Fe oxypnictide systems [5,11,24,25] is remarkably similar to that of the cuprates, for which the high-T_C superconductivity occurs when the antiferromagnetic order of the parent compounds is suppressed by doping. This similarity has inspired a flurry of theoretical and experimental works.

A common behavior for these compounds has emerged in which the stoichiometric parent compound shows a structural transition around 150 K, below which spin-density-wave (SDW) antiferromagnetic ordering [19,20] appears, which is due to nesting Fermi surfaces that are dominated by electronic states of Fe [16]. This SDW ordering is shown to break the degeneracy between the d_{xz} and d_{yz} orbitals of the Fe ion, consistent with the observed tetragonal-orthorhombic structural distortion [22]. Superconductivity occurs when the resistivity anomaly associating with the structural transition is suppressed, which can be achieved in a number of ways such as fluorine doping on the oxygen site [5,11,24,25] or pressure [26,27]. Despite these common features, a wider picture as to how the moment on the lanthanide affects the overall magnetism or why the superconducting transition temperature varies so greatly with different lanthanide ions is still unclear. So far, the magnetic structure has been determined only for LaFeAsO in a system without magnetic rare-earth elements [28]. Thus, it is instrumental to establish whether or not this is a general feature of the $LnFeAsO_{1-x}F_x$ systems.

The $NdFeAsO_{1-x}F_x$ system is the first one to have $T_C \geq 50$ K [8] and now shares the honor with the Ln = Pr, Sm, and Gd compounds [10–12,14]. In this study, we choose NdFeAsO to represent the nonsuperconducting members of the system, and $NdFeAsO_{0.80}F_{0.20}$ the superconducting ones. Polycrystalline samples of 2.6 g NdFeAsO and 7.6 g $NdFeAsO_{0.80}F_{0.20}$ were synthesized using the solid state reaction. We measured resistivity of both samples using the standard four-probe method from pieces from the same batch of samples synthesized for neutron diffraction experiments. The NdFeAsO sample shows a strong anomaly at $T_S \sim 150$ K (Fig. 1), slightly higher than the previously reported value of ~145 K [25], which testifies to the good sample stoichiometry since T_S is known to decrease with doping [25]. The superconducting transition of the $NdFeAsO_{0.80}F_{0.20}$ sample starts at 50 K and reaches zero resistivity at 46 K.

Like in LaFeAsO, the resistivity anomaly is associated with a structural transition at T_S. Powder diffraction spectra of NdFeAsO measured above and below T_S with neu-

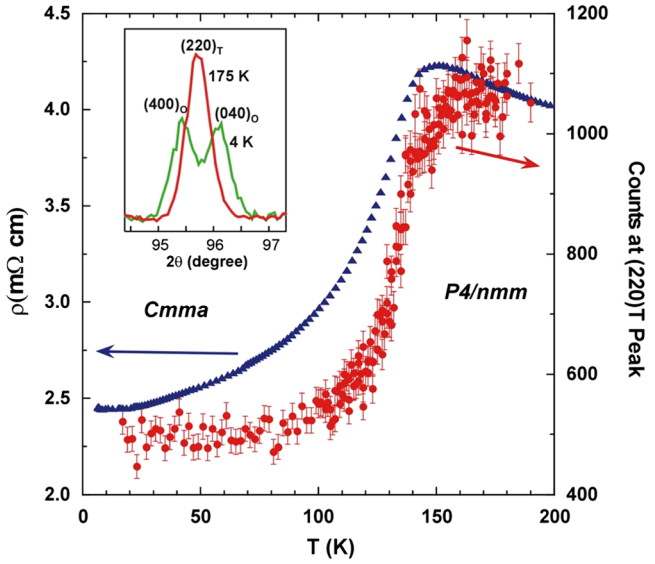

FIG. 1 (color online). Structural transition and its accompanying anomaly in resistivity in NdFeAsO. Both occur at $T_S \approx 150$ K. Above the transition, the crystal has the tetragonal $P4/nmm$ symmetry. Below T_S, the crystal is distorted to have the orthorhombic $Cmma$ symmetry. The transition splits the tetragonal $(220)_T$ Bragg peak into orthorhombic $(400)_O$ and $(040)_O$ peaks as shown in the inset.

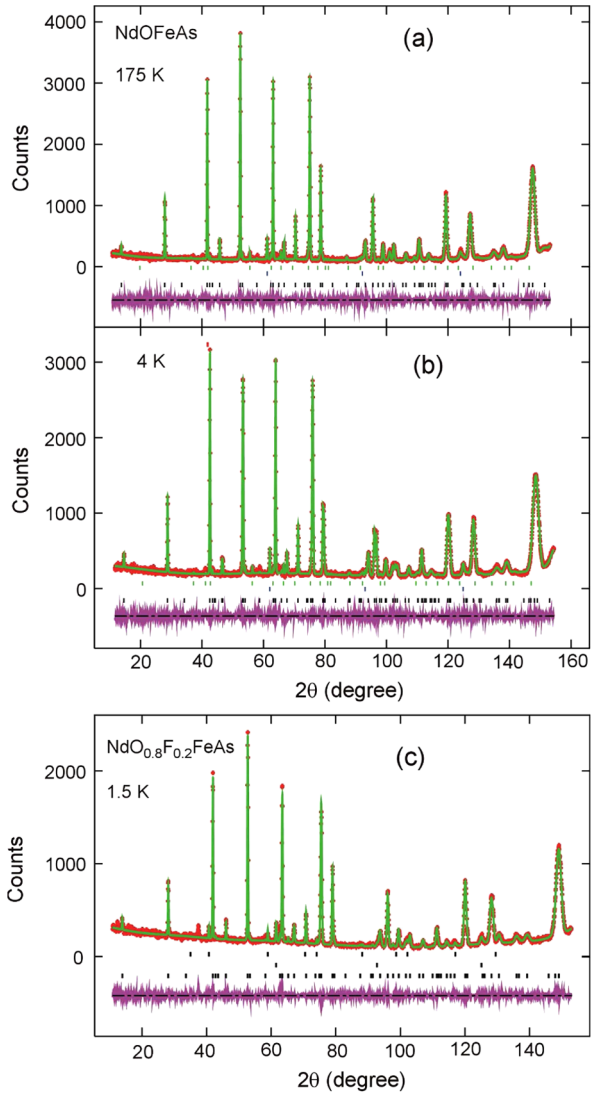

FIG. 2 (color online). Neutron powder diffraction spectra of NdFeAsO at (a) 175 and (b) 4 K, and (c) of $NdFeAsO_{0.80}F_{0.20}$ at 1.5 K. While the spectra in (a) and (c) represent tetragonal symmetry, the spectrum in (b) represents the orthorhombic one.

trons of wavelength $\lambda = 2.079$ Å, using the high resolution powder diffractometer BT1 at the NIST Center for Neutron Research (NCNR), are shown in Figs. 2(a) and 2(b) together with the refined profiles using the GSAS program [29]. The bottom row of vertical bars in the figures indicates the Bragg peak positions of NdFeAsO. The high temperature structure is well described by the tetragonal ZrCuSiAs structure, and the structure parameters at 175 K using space group $P4/nmm$ are listed in Table I. Only small amounts of impurity phases, 3.1% in weight of Nd_2O_3 and 1.3% of Fe, were present in our NdFeAsO sample. The Bragg peak positions of the two impurities are marked by the top two rows of vertical bars, respectively, in the figures. The occupancy of all sites is within 1 standard deviation of the NdFeAsO sample stoichiometry; therefore, the final refinement was performed with the fixed stoichiometric occupancy.

Below T_S, the low temperature structure of NdFeAsO is well accounted for by the orthorhombic space group $Cmma$ as shown by the spectrum at 4 K in Fig. 2(b). In terms of primitive cell parameters (Table I), the distorted structure has $\gamma = 90.296°$, which is almost identical to that of LaFeAsO [28], indicating that replacing La by Nd has almost no effect on the orthorhombic distortion. This is consistent with a recent theoretical study where it was shown that the structural distortion is due to the ordering of the Fe d_{xz}, d_{yz} orbitals in the orthorhombic structure [22]. Similarly, the Fe-As distance is 2.40 Å for both the Nd and La compounds. Discernible difference is in the As-Fe-As angles which are 111.2° and 108.82° for NdFeAsO and 113.99° and 107.06° for LaFeAsO, respectively. It seems that the closer the As-Fe-As angle is to the ideal tetrahedral angle $\arccos(-\frac{1}{3}) = 109.47°$, the higher the T_C.

The orthorhombic distortion doubles the unit cell, which is approximately $(\sqrt{2}a + \varepsilon)(\sqrt{2}a - \varepsilon)c$ in terms of the tetragonal unit cell (Table I). This splits the $(220)_T$ Bragg peak of the tetragonal structure into nonequivalent $(400)_O$ and $(040)_O$ Bragg peaks of the orthorhombic structure; see inset of Fig. 1. To establish the relation between the structural transition and the resistivity anomaly for NdFeAsO, the intensity at the peak position of $(220)_T$ was measured as a function of temperature. As shown in Fig. 1, it is obvious that the anomaly in resistivity is caused by the structural phase transition at $T_S \approx 150$ K, like previously discovered in LaFeAsO [28].

TABLE I. Refined structure parameters for NdFeAsO at 0.3 and 175 K and $NdFeAsO_{0.8}F_{0.2}$ at 1.5 K, respectively.

	NdFeAsO at 0.3 K Space group: *Cmma* $a = 5.6159(1)$ Å, $b = 5.5870(1)$ Å, $c = 8.5570(2)$ Å $V = 268.49$ Å^3 (Prim. Cell: $a = b = 3.9608$ Å, $\gamma = 90.296°$) $R_p = 3.62\%$, $wR_p = 4.86\%$, $\chi^2 = 1.511$								NdFeAsO at 175 K Space group: $P4/nmm$ $a = b = 3.9611(1)$ Å $c = 8.5724(2)$ Å, $V = 134.51$ Å^3 $R_p = 4.95\%$, $wR_p = 6.46\%$					$NdFeAsO_{0.8}F_{0.2}$ at 1.5 K Space group: $P4/nmm$ $a = b = 3.9495(1)$ Å $c = 8.5370(3)$ Å, $V = 133.16$ Å^3 $R_p = 5.74\%$, $wR_p = 7.72\%$				
Atom	Site	x	y	z	B(Å^2)	$M_x(\mu_B)$	$M_z(\mu_B)$	$M(\mu_B)$	Site	x	y	z	B(Å^2)	Site	x	y	z	B(Å^2)
Nd	$4g$	0	$\frac{1}{4}$	0.1389(2)	0.06(5)	1.22(7)	0.96(9)	1.55(4)	$2c$	$\frac{1}{4}$	$\frac{1}{4}$	0.1393(3)	0.29(6)	$2c$	$\frac{1}{4}$	$\frac{1}{4}$	0.1421(4)	0.54(5)
Fe	$4b$	$\frac{1}{4}$	0	$\frac{1}{2}$	0.68(4)	0.9(1)	0	0.9(1)	$2b$	$\frac{3}{4}$	$\frac{1}{4}$	$\frac{1}{2}$	0.61(5)	$2b$	$\frac{3}{4}$	$\frac{1}{4}$	$\frac{1}{2}$	0.12(4)
As	$4g$	0	$\frac{1}{4}$	0.6584(4)	0.97(8)				$2c$	$\frac{1}{4}$	$\frac{1}{4}$	0.6580(4)	1.00(8)	$2c$	$\frac{1}{4}$	$\frac{1}{4}$	0.6599(4)	0.54(5)
O/F	$4a$	$\frac{1}{4}$	0	0	0.56(9)				$2a$	$\frac{3}{4}$	$\frac{1}{4}$	0	0.68(7)	$2a$	$\frac{3}{4}$	$\frac{1}{4}$	0	0.12(4)

There is no structural transition in our superconducting $NdFeAsO_{0.80}F_{0.20}$ sample. The tetragonal ZrCuSiAs structure well describes the observed powder diffraction spectra down to 1.5 K. Figure 2(c) shows the spectrum at 1.5 K together with the refined profile. Only small amounts of impurity phases, 4.4% of NdAs and 1.5% of Fe, were present in the sample. Refined structure parameters at 1.5 are listed in Table I. The lattice of the fluorine-doped $NdFeAsO_{1-x}F_x$ system is more compacted than that of the $LaFeAsO_{1-x}F_x$ system [28,30], and the T_C of the former is higher than T_C of the latter. This trend is consistent with the relation between T_C and pressure [26,27].

Despite the similarity with the structure in NdFeAsO and LaFeAsO, we did not observe the SDW order of the type observed in LaFeAsO with the magnetic wave vector $(1/2, 1/2, 1/2)_T$ [28] in either our NdFeAsO sample down to 1.5 K or the $NdFeAsO_{0.80}F_{0.20}$ sample down to 6 K, using BT1 or higher flux triple-axis spectrometer BT9 or BT7 at the NCNR. Our measurements at BT9 and BT7 set the upper limit for the staggered magnetic moment of the LaFeAsO-like SDW order at below $0.17\mu_B$/Fe at 30 K for NdFeAsO and below $0.08\mu_B$/Fe at 45 K for $NdFeAsO_{0.80}F_{0.20}$. In fact, all-electron first-principles calculations, similar to one in Ref. [22] but using the LaFeAsO structure with the lattice parameters of NdFeAsO, show that the Fe moment is reduced from $0.48\mu_B$ for La to $0.30\mu_B$ for Nd system. Since the Bragg intensity is proportional to the square of the ordered moment, this suggests about 1/3 intensity decrease in NdFeAsO compared to the La system, providing a possible explanation of why we did not observe the $(1/2, 1/2, 1/2)_T$ type of SDW order in NdFeAsO.

Instead, a new type of the long-ranged magnetic order with wave vector $(1/2, 1/2, 0)_T$ was observed below 2 K in NdFeAsO. In Fig. 3, neutron powder diffraction spectrum measured at BT1 at 0.3 K for the NdFeAsO sample in a ^{3}He cryostat is shown. When compared to the spectrum taken at 4 K in Fig. 2(b), additional magnetic Bragg reflections are visible. They are highlighted in the inset and marked by the vertical lines. In Fig. 4, the temperature dependence of the magnetic Bragg peak $(100)_O$, measured at BT7, is shown. The solid line represents the mean-field theoretical fit for the squared magnetic order parameter, and the Néel temperature is determined as $T_N = 1.96(3)$ K.

The magnetic wave vector $(1/2, 1/2, 0)_T$ of the low temperature antiferromagnetic order in NdFeAsO is consistent with the orthorhombic crystal structure below T_S. Therefore, there is no further crystal symmetry breaking below T_N. The parallel alignment of magnetic moments along the c axis demanded by the magnetic wave vector in NdFeAsO differs from the antiferromagnetic one in LaFeAsO, which further doubles the unit cell along the c axis. The low $T_N = 1.96(3)$ K indicates the important role played by Nd in the antiferromagnetic transition, as rare-earth magnetic ions often order at low temperature, such as in the high-T_C cuprate $Nd_{2-x}Ce_xCuO_4$ system below ~1.2 K [31,32]. However, a magnetic model with Nd ions alone cannot account for the magnetic diffraction pattern; see Fig. 5. We solved the magnetic order using a combined Nd and Fe antiferromagnetic structure. Comparison of the Rietveld refinement fits to magnetic models with different moment directions and the directions of the ferroalignment and antiferroalignment of the moments clearly shows significantly better result for the

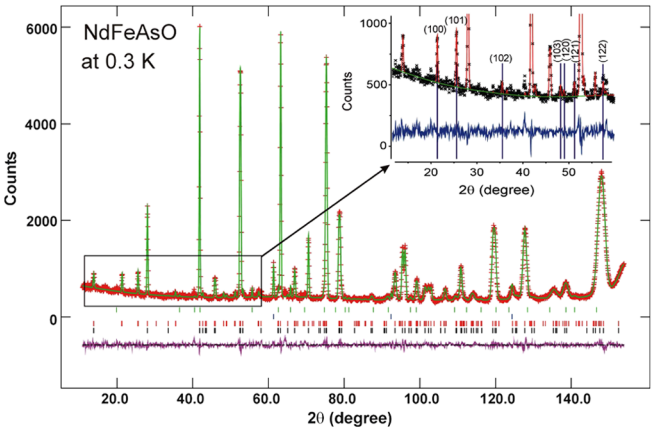

FIG. 3 (color online). Neutron powder diffraction spectrum at 0.3 K. The small angle part is magnified in the inset, and magnetic Bragg peaks which are absent at 4 K are marked by the vertical lines and are indexed using the orthorhombic *Cmma* unit cell.

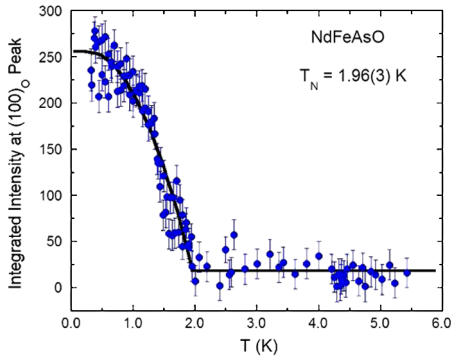

FIG. 4 (color online). The intensity of magnetic Bragg peak $(100)_O$ as a function of temperature.

model shown in Fig. 5. The resulting crystalline and magnetic refinement is shown in Fig. 3, and the structure and magnetic parameters at 0.3 K are listed in Table I. The Fe moments are orientated along the longer of the two axes, a, the direction where Nd also has a component. While the antiferromagnetic alignment for Nd is along the b axis, it is along the a axis for the Fe moments, which is consistent with previous first-principles calculations [22]. The total staggered magnetic moments are $1.55(4)\mu_B$ per Nd and $0.9(1)\mu_B$ per Fe at 0.3 K.

In summary, we presented a detailed neutron diffraction study of the structural and magnetic properties of NdFeAsO and the doped 50 K superconductor $NdFeAsO_{0.80}F_{0.20}$. We clearly show that NdFeAsO and LaFeAsO systems have very similar structural properties. The Nd system is more compacted and its FeAs tetrahedron is closer to the ideal than the La system. We were not able to observe the LaFeAsO-like SDW ordering below T_S, suggesting a weaker SDW instability in NdFeAsO. Below 1.96 K, parallel Fe moments on a bc plane with a sizable saturated moment $0.9\mu_B$ alternate along the a axis in a combined magnetic order with Nd moments, whose in-plane magnetic wave vector is the same as the SDW nesting vector. From our results, it is tempting to conclude that the reason for the higher T_c in NdFeAsO is the different structure parameters due to smaller lanthanide ion (Table I) and not due to other effects.

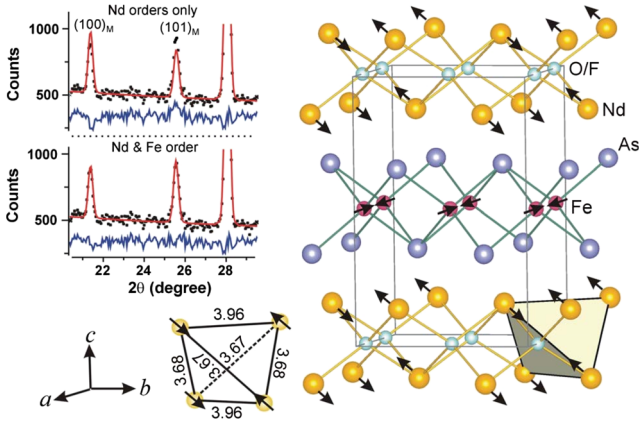

FIG. 5 (color online). Magnetic structure of NdFeAsO below $T_N = 1.96$ K in the orthorhombic unit cell. The Nd tetrahedron structure element is also shown. A comparison of the Rietveld refinement fits using a Nd only model as compared with a Nd/Fe coupled model is included to highlight the necessity for the latter to fully describe the magnetic order.

Work at LANL is supported by U.S. DOE-OS-BES, at USTC by the Natural Science Foundation of China, Ministry of Science and Technology of China (973 Project No. 2006CB601001), and by National Basic Research Program of China (2006CB922005).

*wbao@lanl.gov

[1] Y. Maeno *et al.*, Nature (London) **372**, 532 (1994).
[2] M. J. Geselbracht *et al.*, Nature (London) **345**, 324 (1990).
[3] K. Takada *et al.*, Nature (London) **422**, 53 (2003).
[4] E. Morosan *et al.*, Nature Phys. **2**, 544 (2006).
[5] Y. Kamihara *et al.*, J. Am. Chem. Soc. **130**, 3296 (2008).
[6] X. H. Chen *et al.*, Nature (London) **453**, 761 (2008).
[7] G. F. Chen *et al.*, Phys. Rev. Lett. **100**, 247002 (2008).
[8] Z. A. Ren *et al.*, Europhys. Lett. **82**, 57 002 (2008).
[9] Z. A. Ren *et al.*, Mater. Res. Innovations **12**, 105 (2008).
[10] Z. A. Ren *et al.*, Chin. Phys. Lett. **25**, 2215 (2008).
[11] R. H. Liu *et al.*, Phys. Rev. Lett. **101**, 087001 (2008).
[12] Z.-A. Ren *et al.*, Europhys. Lett. **83**, 17 002 (2008).
[13] Z. A. Ren *et al.*, Supercond. Sci. Technol. **21**, 082001 (2008).
[14] C. Wang *et al.*, Europhys. Lett. **83**, 67 006 (2008).
[15] S. Lebegue, Phys. Rev. B **75**, 035110 (2007).
[16] D. J. Singh and M.-H. Du, Phys. Rev. Lett. **100**, 237003 (2008).
[17] K. Haule *et al.*, Phys. Rev. Lett. **100**, 226402 (2008).
[18] C. Cao *et al.*, Phys. Rev. B **77**, 220506(R) (2008).
[19] F. Ma and Z. Y. Lu, Phys. Rev. B **78**, 033111 (2008).
[20] J. Dong *et al.*, Europhys. Lett. **83**, 27 006 (2008).
[21] I. A. Nekrasov *et al.*, JETP Lett. **87**, 560 (2008).
[22] T. Yildirim, Phys. Rev. Lett. **101**, 057010 (2008).
[23] P. W. Anderson, Science **235**, 1196 (1987).
[24] H. H. Wen *et al.*, Europhys. Lett. **82**, 17 009 (2008).
[25] G. F. Chen *et al.*, Chin. Phys. Lett. **25**, 2235 (2008).
[26] H. Takahashi *et al.*, Nature (London) **453**, 376 (2008).
[27] W. Lu *et al.*, New J. Phys. **10**, 063026 (2008).
[28] C. de la Cruz *et al.*, Nature (London) **453**, 899 (2008).
[29] A. Larson and R. B. Von Dreele, GSAS: Generalized Structure Analysis System (1994).
[30] Y. Qiu *et al.*, Phys. Rev. B **78**, 052508 (2008).
[31] J. W. Lynn *et al.*, Phys. Rev. B **41**, 2569 (1990).
[32] R. Sachidanandam *et al.*, Phys. Rev. B **56**, 260 (1997).